Imaging plasmas with coded aperture methods instead of conventional optics

by

Pakorn Wongwaitayakornkul

Summer Undergraduate Research Fellowships 2012, Caltech

Mentor: Paul Bellan

Abstract

The spheromak and astrophysical jet plasma at Caltech emit localized EUV and X-rays associated with magnetic reconnection. However, conventional optics does not work for EUV or X-rays due to their high energy. Coded aperture imaging is an alternative method that will work at these energies. The technique has been used in spacecraft for high-energy radiation and also in nuclear medicine. Coded aperture imaging works by having patterns of materials opaque to various wavelengths block and unblock radiation in a known pattern. The original image can be determined from a numerical procedure that inverts information from the coded shadow on the detector plane. A one-dimensional coded mask has been designed and constructed for visualization of the evolution of a 1-d cross-section image of the Caltech plasmas. The mask is constructed from Hadamard matrices. Arrays of photo-detectors will be assembled to obtain an image of the plasmas in visible light range. The experiment will ultimately be re-configured to image X-ray and EUV radiation.

1. Introduction

1.1 The classical methods of 2d imaging

An image is a mapping over space of distribution of photon emitter. At high energy of photon radiation, diffraction can be neglected and geometric optics used with excellent approximation. (Accorsi 2001). Classically, there are two devices used to create such mapping: pinhole and collimator. Both procedures generate one-to-one correspondence between detector and object.

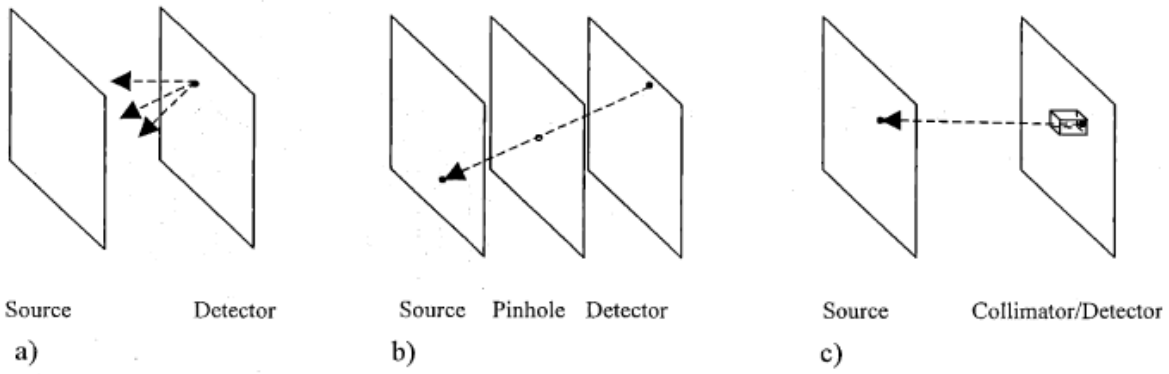

Figure 1: (a) if no imaging system is present, a count collected at the detector cannot be traced back to any specific part of the source. A pinhole (b) and a collimator (c) establish a one-to-one correspondence between detector and object. With a geometrical construction one can associate each detected event with an emission location.

1.2 Why a coded aperture

The main problem in using pinhole and collimator is that the intensity of photon detected per unit area is fairly small, if small hole is used. However, increasing the size of the hole would result in losing of resolution. Therefore, using coded aperture, which is basically a collection of pinhole camera in a specific pattern, is an attempt to achieve the resolution of small pinholes while maintain a high signal throughput.

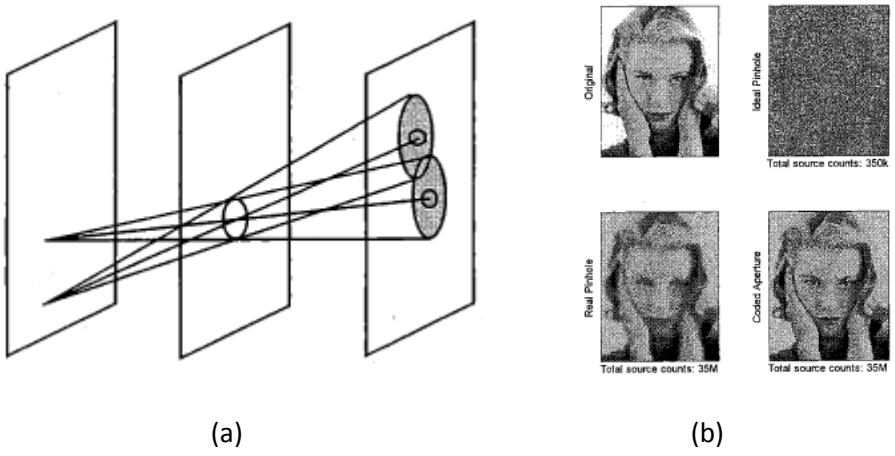

Figure 2: (a) Resolution loss when an ideal pinhole is enlarged to increase throughput. (b) Intuitive visualization of the trade-off between noise and resolution for pinhole and collimator imagers

Another significant benefit for coded aperture imaging is that, unlike conventional optics, it allows imaging of high energy radiation. Mirrors and lens that are often used in the lab are not able to focus photon at high energy.

1.3 Related papers and plasma imaging

To observe cosmic ray, two types of telescope are usually used: reflection mirror and mask-type. The first kind only works within a certain range of wavelength, i.e. light with energy below 3 keV, because of the poor reflectivity of the mirror at higher energy of light (Miyamoto, Hadamard Transform X-ray Telescope 1977). To record image of light outside the range such as EUV or X-ray, the mask type is needed. Coded aperture imaging (CAD) is a mask-type technique in astronomy used to detect high-energy radiation by having patterns of materials opaque to various wavelength of light block and unblock light in a known pattern. Then using computer algorithm, one can deduce the properties of the original light from a coded shadow upon a plane of detector. Hadamard transformation is a widely used algorithm which increases signal to noise ratio of the observed signal (Miyamoto, Hadamard Transform X-ray Telescope 1977). Therefore, this method could be applicable to do EUV or X-ray imaging of plasma in the lab at Caltech. The principle of the Hadamard transform was originally used in X-ray telescope, but it is also related to other fields such as plasma diagnosis by emission X-rays and medical diagnosis by gamma rays. For example, there are medical diagnosis methods described by Akcasu et al. (Akcasu, et al. 1974) and Koral et al. (Koral, Rogers and Knoll 1975).

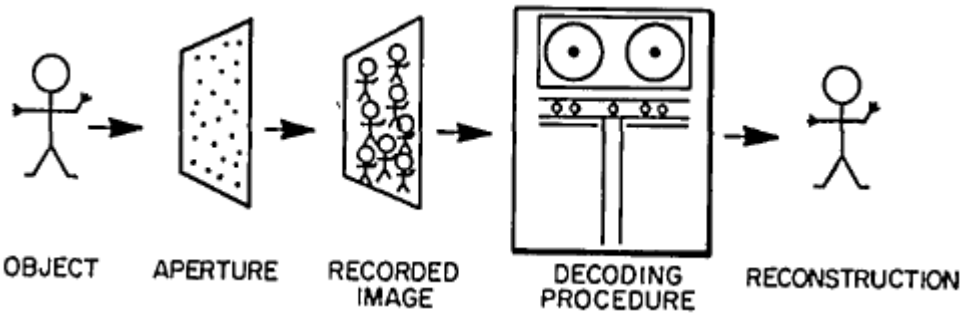

Figure 3: The basic steps involved in coded aperture imaging (Fenimore and Cannon 1978).

The successful mask allows us to do EUV or X-ray imaging. In this case, one-dimension analysis should be enough. When we record images in a different time, we should be able to assemble all the images to make 2-dimensional picture of plasma that passes through a plane. This would help us understand more characteristics of Spheromaks and astrophysical jets from its EUV or X-ray image that could not be detected using lens or mirrors.

2. Approach

First, a simple experiment to test the algorithm to decode for the original signal was set up. As shown in figure 4, a shadowed pattern on the detector can indicate where the light source is. The source is an Iphone's flash and the detector is a multichannel array photodetector, which works well in the visible light range, with 16 elements. Since there only exists PN-sequence[1] of length 15, but not 16, I only used 15 elements of the detector. PN-sequence and a row of a core of cyclic Hadamard matrix are closely related (Nelson and Fredman 1970).

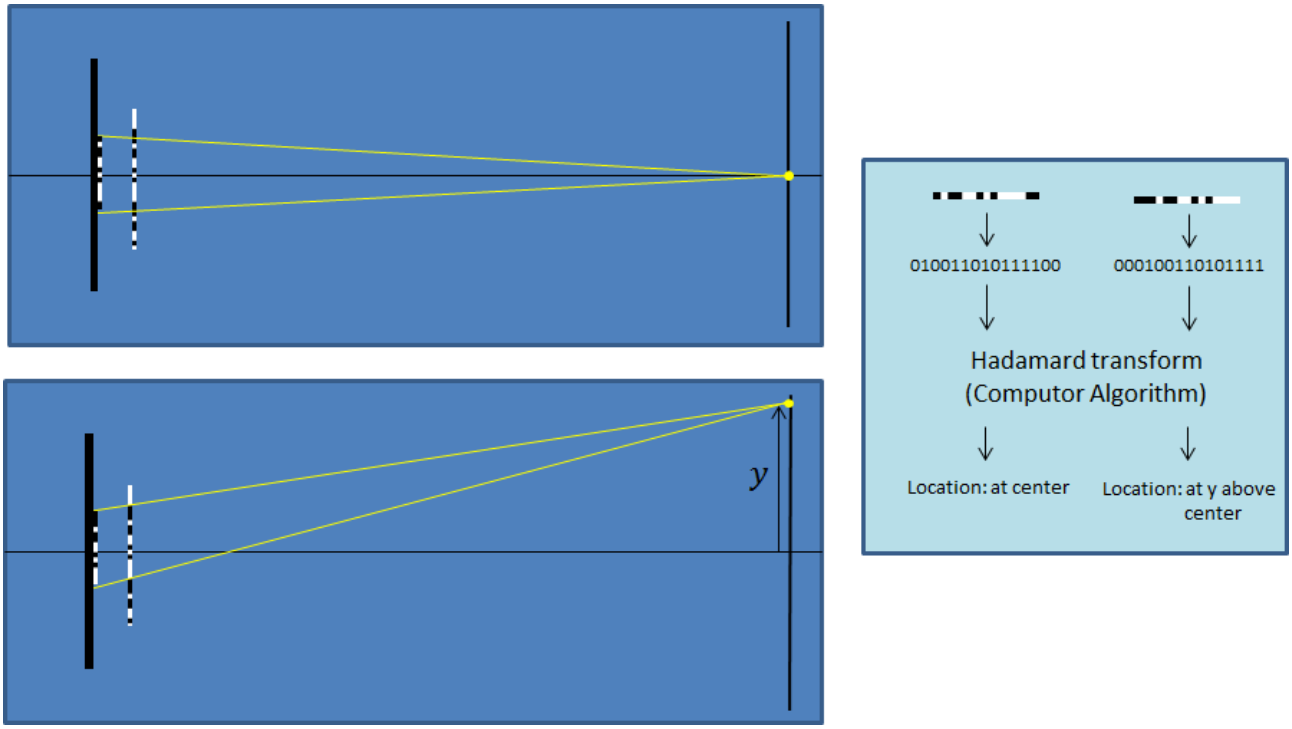

Figure 4: Illustration of using Hadamard transformation to determine a location of the light source

In this setting, light was assumed to come from infinity, so a dimension of an element of the mask was set to be the same as that of the detector. The mask is made from printing pattern onto a transparent overhead paper. For the assumption to be valid, the distance between the light source and the mask should be much greater than that between the mask and the detector. Also note that the current from voltaic effect is very small; therefore, the current amplification circuit was required.

Below is a result of Hadamard transformation. The signal received by the detector might seem random. (It is actually the pattern of the designed mask). However, after being transformed, the detected signal appeared to be a nice single-peak original signal as seen in figure 5.

[1] PN-sequence stands for Pseudo-Noise sequence. It is a sequence of binary number that seems to be random, but actually deterministic (Golomb, 1964).

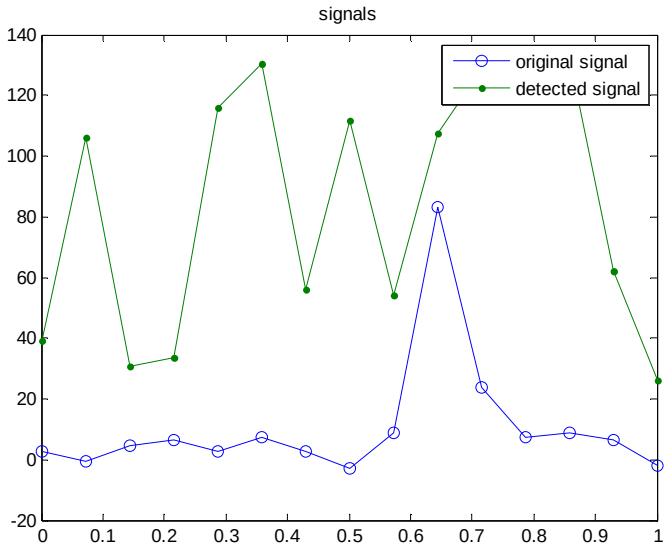

Figure 5: The graph of original signal and detected signal

To observe resolution of the image, light source was located at y = -20, -10, 0, 10, and 20 cm. A parameter y is defined in figure 4. As shown in figure 6, the location of the peaks is shifted with a small decrease in its intensity.

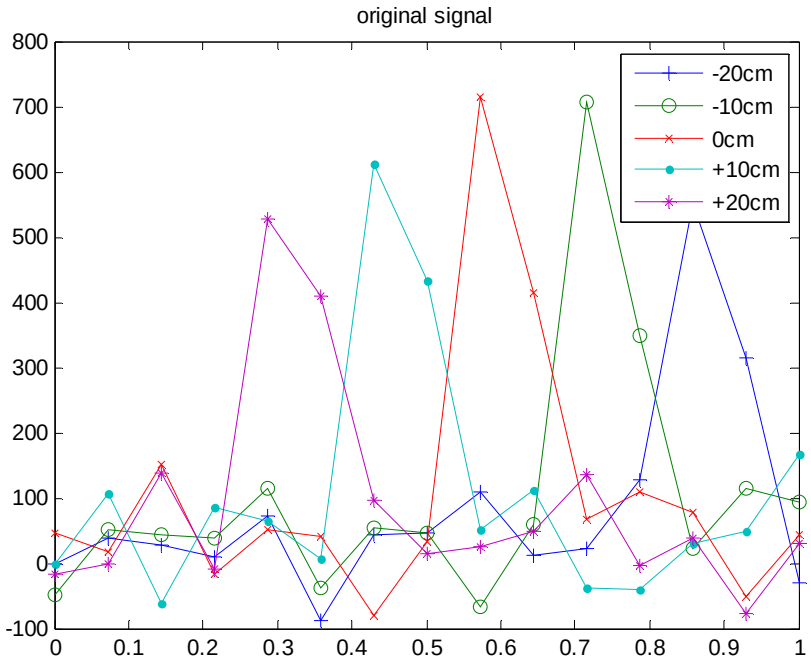

Figure 6: graph of original signal where the labels are the values of y in figure 4

Next, this method was used to capture the visible light image of plasma of size 5 cm with 1 mm size of each pixel. To do so, the number of element of the detectors was increased to be 47

elements. This can be obtained by mounting three of them end to end to each other (47 was used instead of 48 for the same reason 15 was used, not 16). Also the mask was expected to be far from the light source at least a meter, since the mask must be put outside of the plasma chamber and a meter is approximately how big the chamber is in radius. Additionally, now the size of the element of the mask should not be the same with that of the detector, since assumption of parallel light is no longer true. However, the sizes can be calculated by the condition that each point of light source should be able to project one cycle of mask (47 elements) into the detectors. From all of these conditions, calculated geometry was set to be: distance between mask and detector = 1.59 m, distance between mask and plasma = 1.00 m, size of an element of detector = 0.0625 inch, size of an element of mask = 0.0242 inch.

While working on the experiment, some papers associated with coded aperture imaging were collected. There are several good papers about such as Signal-to-noise ratio in coded aperture imaging (Shutler 2012), Coded aperture imaging with uniformly redundant arrays (Fenimore and Cannon 1978), Some Characteristic of the Hadamard Trasnform X-ray Telescope (Miyamoto, Tsunemi and Tsuno, Some Characteristic of the Hadamard Trasform X-ray Telescope 1981) and Scatter-hole cameras for X-ray and Gamma rays (Dicke 1968). These are excellent resource for understanding more about the concept of CAD.

After the code for Hadamard Transformation was verified and new geometry for setting is calculated, a PN-sequence of length 47 is **not** in the form of $2^n - 1$, where n is an integer. Such sequence must then be generated with other method. Fortunately, there exists PN-sequence of period 47 of a type Legendre sequence and it could be determined (Baumert 1964). An image of mask generated from that sequence is shown below.

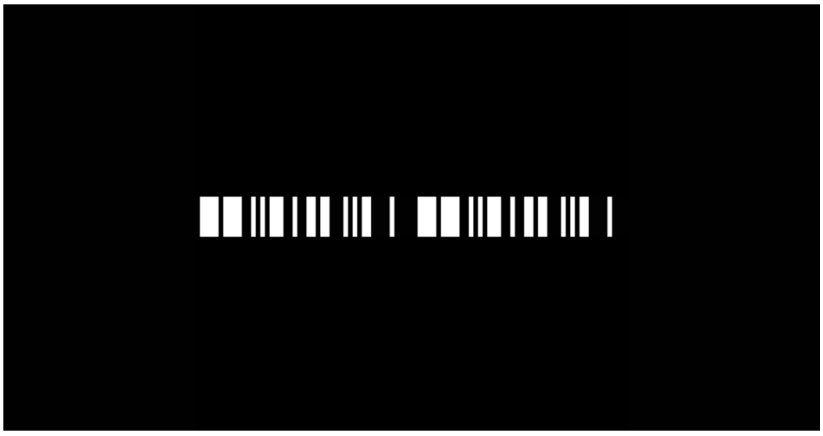

Figure 7: mask pattern generated from PN-sequence of period 47

Originally, a laser was chosen as a light source to increase the intensity of the signal and then used lenses to increase the diameter of the laser beam. It turns out that using lenses would not work because it did not uniformly distribute light in every direction. The laser light has a largest intensity at the center and smaller intensity away from the center. This violates our assumption that a point source emits light uniformly in any direction. Therefore, an Iphone's flash was already a good choice but this time increases the resistance used in the amplifier to be around 20 Mega-ohms. This should increases the signal we get by a factor of 4. Below is the graph of the detected signal and original signal. As expected, the original signal is a nice single peak.

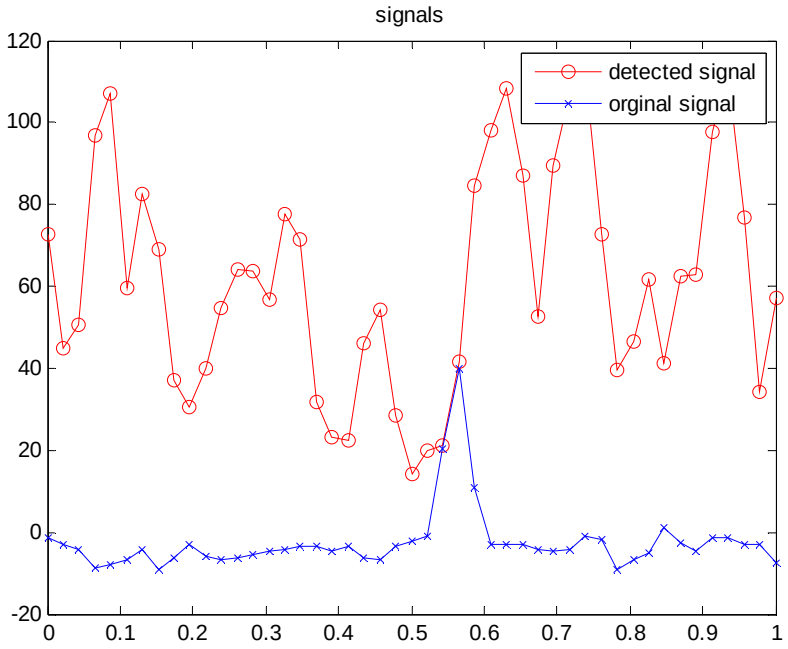

Figure 8: graph of detected and its inverse signal

Consequently the resolution of our system was checked. Using a base as shown in Fig.9, light source can be adjusted by the smallest increment of 0.001 inch.

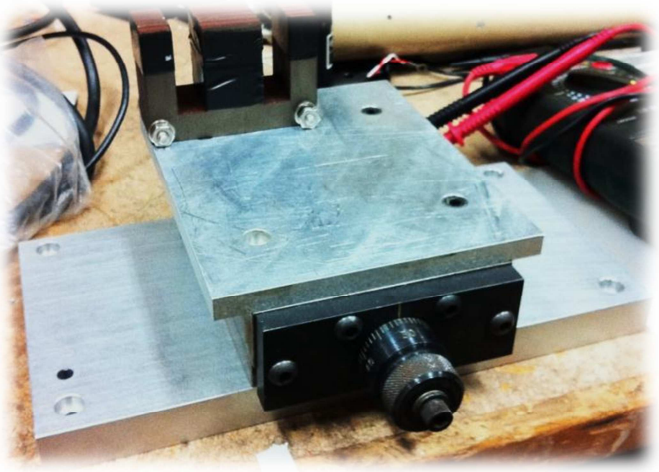

Figure 9: the base with the smallest increment of 0.001 inch

Then the source was moved by 0.04 inches, which is roughly around 1 mm (our desired resolution). As expected, the peak is shifted by 1 unit each time we move our source by 1 mm as shown in Fig.10.

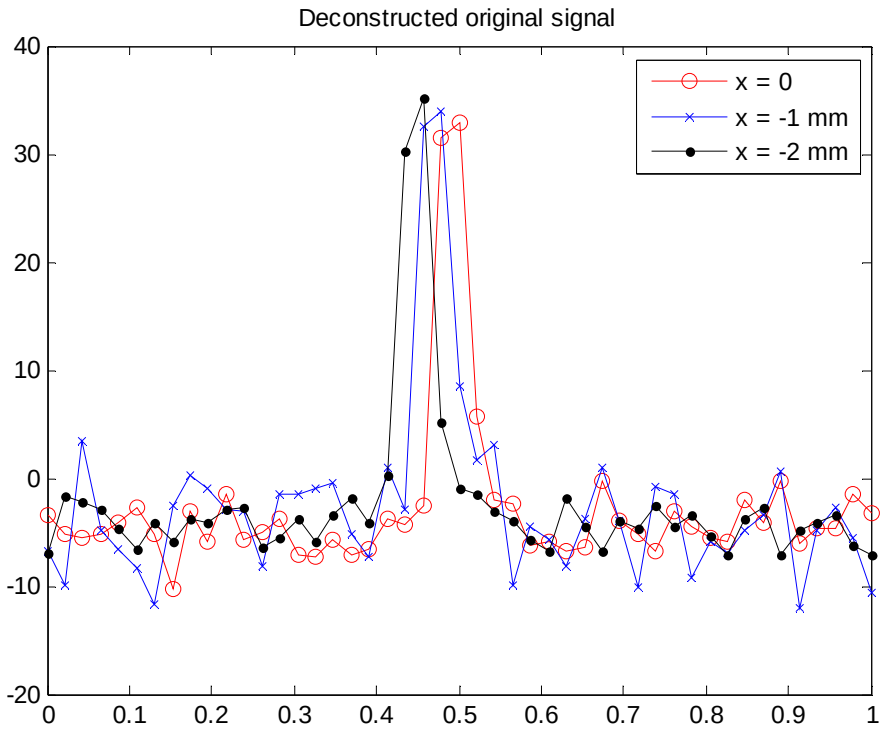

Figure 10: we can see the shift of the peak by 1 unit each time we moved the source by 1 mm

Next step is to test if the photo-detector alone without an amplifier would be able to produce enough signals for the diagnostic. If not, making 47 amplifier circuits would be possible

but quite troublesome and time consuming. To check this, a photo-detector was mounted to a camera stand and a laser pointer was used to aim that the photo-detector was actually pointing to the location of the plasma. The experiment was performed on the spheromak side with Ar gas. Fig. 11 is a diagram illustrating three locations of the detector. Location A is around 1.5 meter away from the window, while location B is a little closer and location C is a little further.

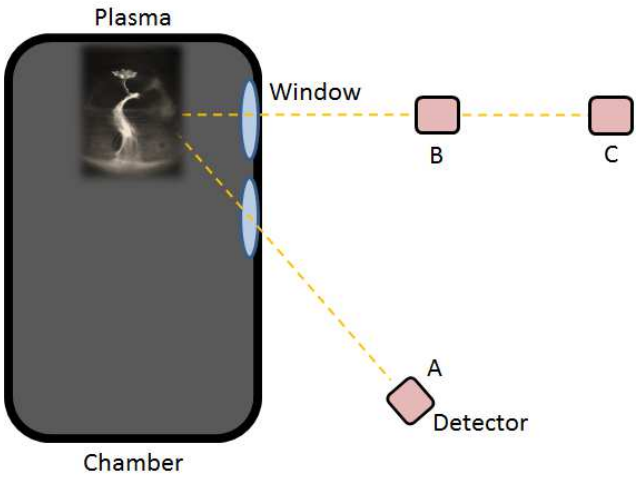

Figure 11: Diagram illustrates the location of the detector respecting to the chamber

Below is the result from collecting several shots at different condition. Figure 11(a) is a shot that was taken at the location A. So is figure 11(b) but in 11(b) PFN[2] is turned on. As expected, in 11(b) the signal last longer than 11(a). Then figure 11(c) and 11(d) are shots without PFN at the location B and C respectively. At location B, the signal peak is approximately at 0.06 mA, while at location C, the signal peak is at around 0.2 mA. Note that all of the signals shown below are detected without a mask being placed in front of the detector. Putting a mask in front would reduce the detected signal by roughly 50%.

[2] Pulse forming network

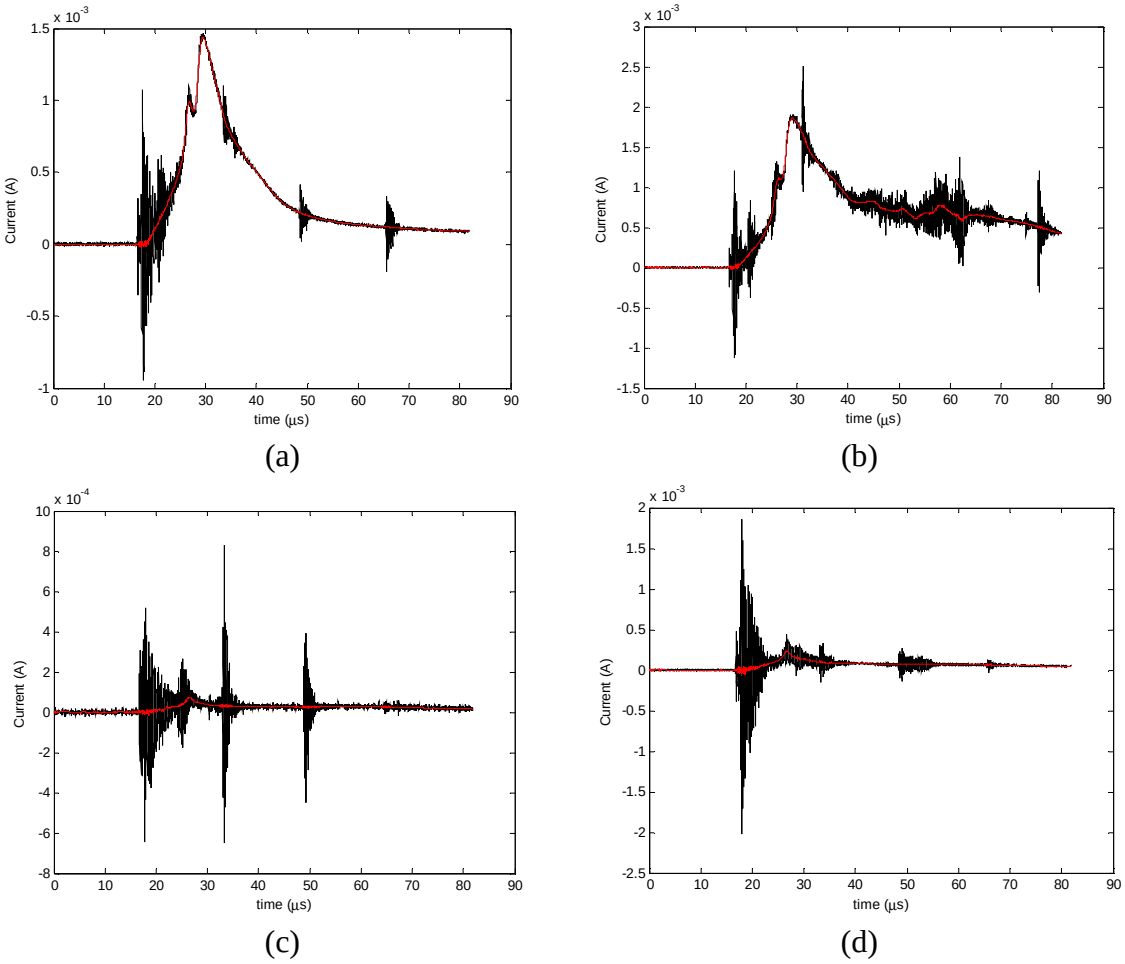

Figure 12: Signals received by the detector at the different location

As a result, a small signal from the detector can be detected at desired location (probably somewhere in between B and C). The signal is quite small, but we will try to use detector alone without amplifiers for now and see if we obtain a good enough image. The following step would be to construct an aluminum box to mount photo-detectors with 48 BNC-connectors as sketched in the drawing below. Then use this to image the plasma with mask.

Next, a metal box which contains 48 arrays of photodiode was constructed. Each element of photodiode array was connected via BNC cable into lab's VME digitizer. The trigger was set to be the same trigger as plasma gun through an optical cable. All 48 arrays connected to 48 channels in 6 VME digitizers. The signals then were processed and saved using IDL code. New IDL subroutine was written to collect all signals at each discretized time. Matlab was then used to deconstruct and plot the original image.

Before put in the mask, image detection of the metal box with 47 VME channels can be checked using a single pinhole. Having this result, we can scope what to expect from the case with the mask. Note that the experiment is performed at a closer distance than what we expected to when using the mask. There are two main reasons behind. First the signal level might tremendously drop because of decreasing in area of transmission. Second the range of horizontal field of view would be wider. As a result the full shape of plasma can be captured. The figure 13 below is a collection of such results. Additionally, in figure 13(c) and 13(d), the detector is moved to position at angle, i.e. similar to position A in figure 11, but closer.

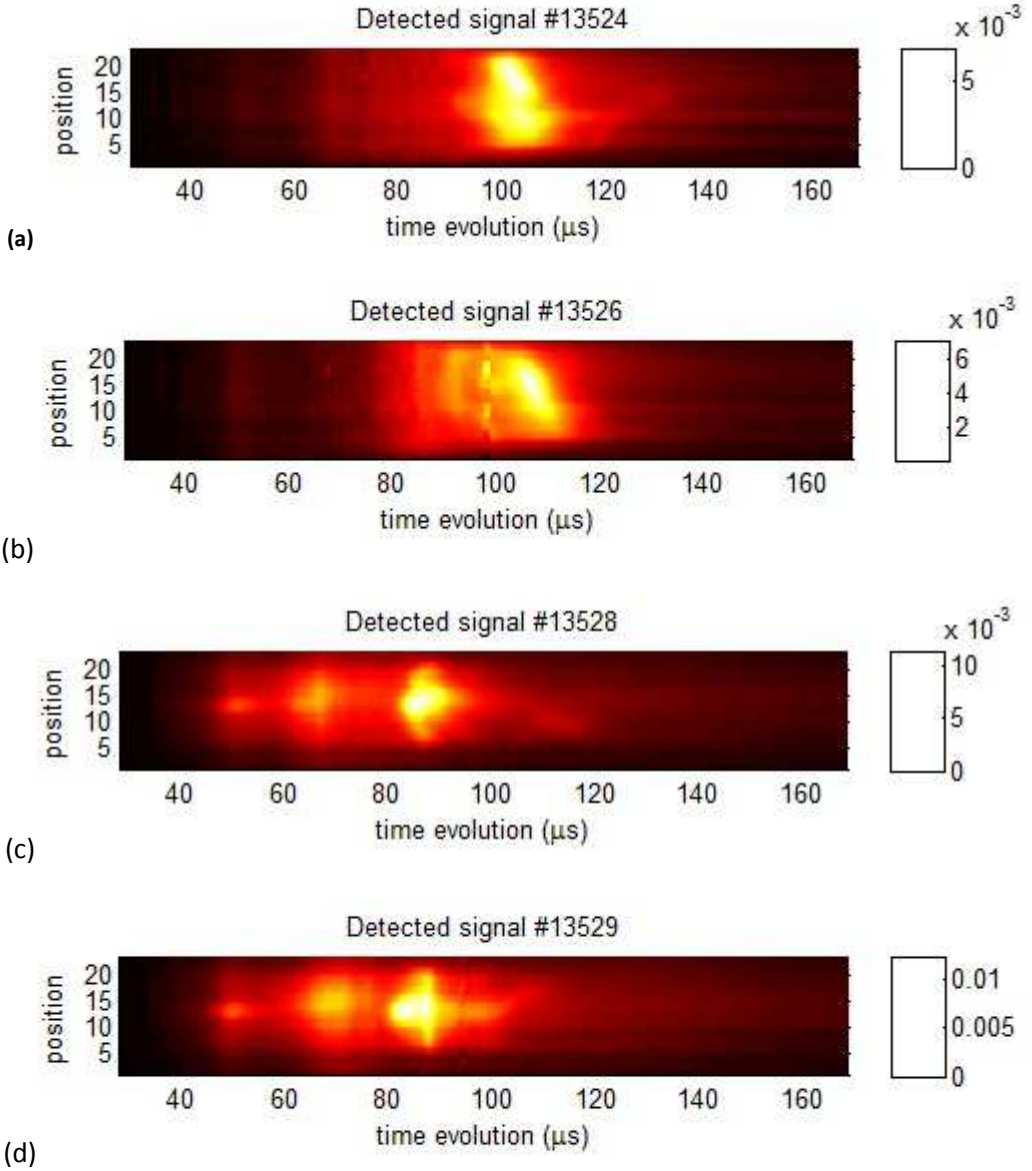

Figure 13: Collections of plasma images obtain from pinhole camera using metal box detector (a)&(b) at perpendicular view (c)&(d) at some angle

Lastly, the detector was placed at the distance specified in page 6. The mask was also placed at a specific position in between the plasma and the detector. A Matlab code was written to deconstruct plasma image using signal from VME digitizer. Figure 14 shows a result.

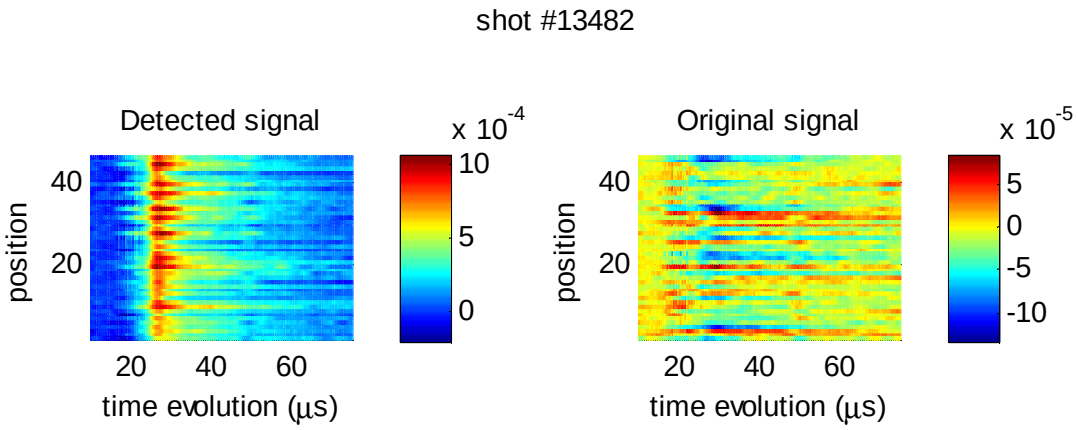

Figure 14: Image of the detected signal and transformed signal of Ar gas using CB only

Below in figure 15 is another shot taken in this setting. In this shot, the detector was shifted upward, so the shift in plasma image was expected. However, such change was not noticeable here.

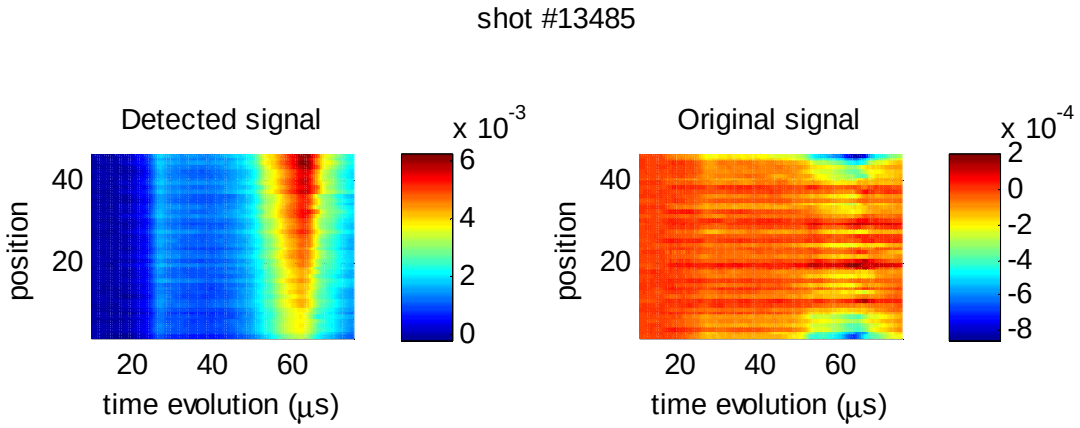

Figure 15: Image of the detected signal and transformed signal of a shot CB+PFN of Ar gas when the detector is lifted upward

In conclusion, the bench-test experiments went well with satisfying results. The graph of each one was a nice delta function as the source is a single point light source. The required resolution of 1 mm was also achieved. Furthermore, the metal box was able to capture plasma using pinhole camera. Its shape looked reasonable comparing to the pictures taken with Imacon camera.

However, the inversed signals from metal box detector through the mask do not resemble any shape of plasma, as shown in figure 14 and 15. This bizarre result could come from the Matlab code since it was quite a big leap to jump from imaging single point light source to plasma image. Nonetheless, the mistake in Matlab code is yet to be found. Another possibility was that the setting somehow violated some assumptions, which could arise to problems. Unfortunately, the end of summer arrived and there was not enough time to figure out the mistake. The author hopes that the investigation of CAD including the equipment made and code written would be helpful for further CAD examination in Bellan Lab.

3. Method

3.1 Mathematical construction

Hadamard transform is widely used in Hadamard spectroscopy and Hadamard matrix plays a significant role in the transformation. By definition, a Hadamard matrix is a square matrix whose elements are 1 and -1 and whose row vectors are mutually orthogonal, i.e. $HH^T = nI_n$, where I_n is a n-by-n identity matrix. From its property, one can investigate normalized Hadamard matrix, which is a Hadamard matrix whose first row and column only contain 1. The matrix part where the first row and column are excluded is called core of normalized Hadamard matrix. Moreover, if each row of the core is just the first row shifted, then it is called cyclic Hadamard matrix. Examples of normalized Hadamard matrix and cyclic Hadamard matrix are shown in figure 16 below.

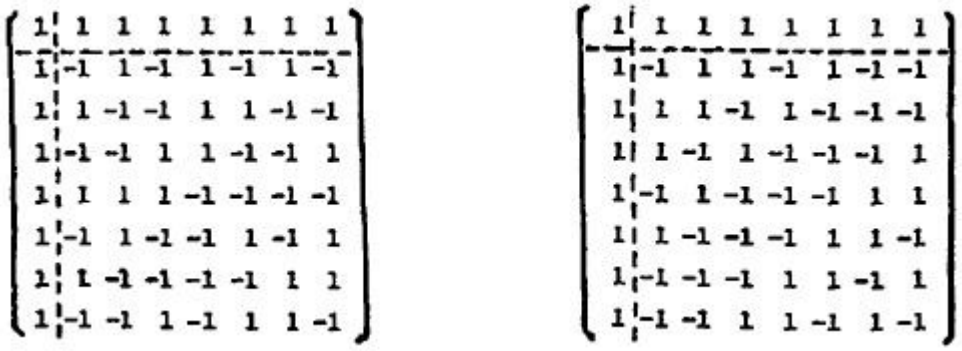

Figure 16: (Left) Normalized Hadamard matrix. (Right) Cyclic Hadamard matrix.

Next the variables used in the mathematical construction are defined as follow:

H_c - Core of $(N+1) \times (N+1)$ cyclic Hadamard matrix

M - Mask matrix. Obtain from H_c by changing -1→1 and 1→0, i.e. $\mathrm{M} = \left[\frac{1}{2}(U - H_c) \right]$

D - Detected signal vector of length N

F - Original signal vector of length N

F_R - Reconstructed signal vector of length N

First detected signal is transformed through matrix M by (This is what happen when signal goes through the mask).

$$D = M^T F$$

Then if one considers the product of $H_c M^T$, it ends up being a multiple of identity matrix.

$$H_c M^T = H_c \left[\frac{1}{2}\left(U - H_C{}^T\right) \right] = \frac{1}{2}[-(N+1)I]$$

Finally, one can transform the signal back using matrix multiplication as shown below.

$$F_R = -\frac{2}{N+1} H_c D = -\frac{2}{N+1} H_c M^T F = \mathrm{F}$$

■

3.2 Set up for first bench-test experiment

On the first bench-test experiment, multichannel array photodiode, as shown in figure 17, was used as a detector. The photodiode contained 18 pins: 16 for each channel and 2 for ground. Light source was an Iphone's flash. Since its intensity was not in a detectable range, an amplifier circuit (current-voltage converter) was assembled.

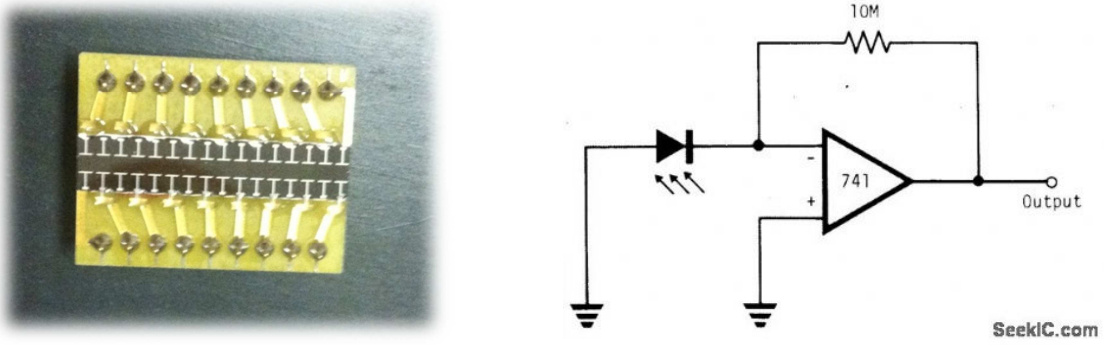

Figure 17: Multichannel array photodetector with 16 elements and diagram for amplifier circuit

The mask was made from a transparent printing paper, normally being used with overhead projector. The pattern was generated from PN-sequence with periodicity 15 (Nelson and Fredman 1970) then was designed in Photoshop and printed from laser printer. Figure 18 shows the created mask comparing with its design from computer. In addition, on the design,

there were binaries labeled under the mask so as to demonstrate relation between the pattern and its PN-scquencc.

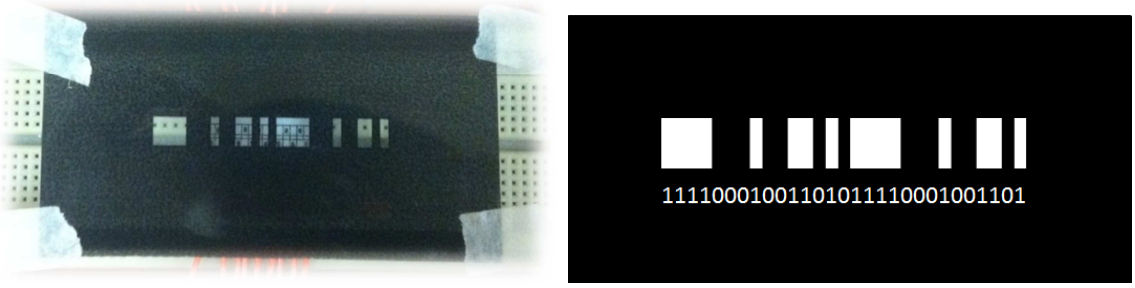

Figure 18: Mask pattern and its corresponding PN- sequence

Figure 19 are photos of complimentary amplifier circuit and a breadboard where everything was put together. An op-amp was powered by two 9V batteries. Only one amplifier was created to manually measure signal from each channel. The light source (Iphone) was placed roughly a meter away from the board.

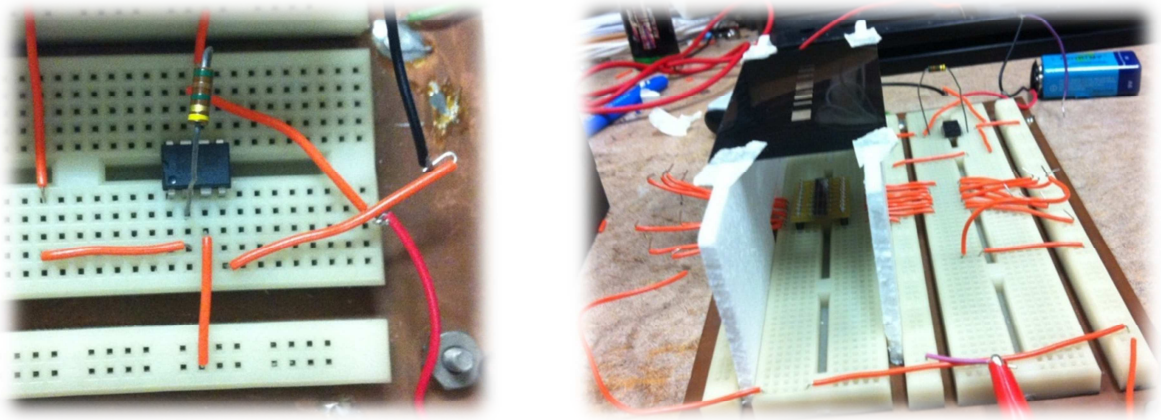

Figure 19: Amplifier circuit and set up altogether

3.3 Geometry determination for specified resolution

In this section, the method of determining geometry of mask, distance between object-mask, and mask-detector will be discussed. First let label some variables. Let size of an element of object, mask, and detector to be $l, m,$ and d respectively. a and b denote distance as illustrated in figure 20.

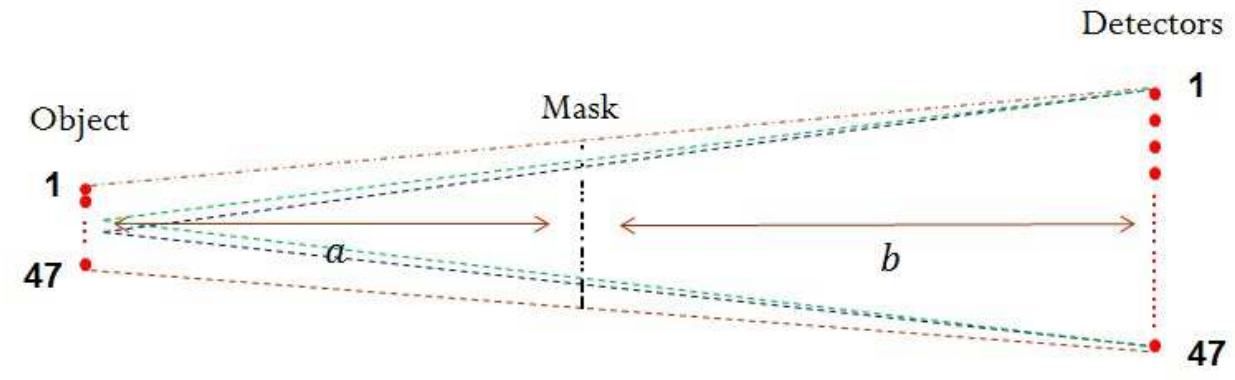

Figure 20: Diagram illustrates the geometry of object-mask-body system

To archive our specified resolution, requirements are

1. Light from each object point must cover exactly 1 cycle of mask before reaching the detector. This can be translate into equation as $\frac{a+b}{a} = \frac{d}{m}$.
2. Two point sources that are 1 mm away in the object should cover the almost the same pattern (same pattern but shifted by one element). This condition simply implies that the resolution of the image is 1 mm. This equation follows: $\frac{a+b}{b} = \frac{1\,\text{mm}}{m}$. $[l = 1\,\text{mm}]$
3. Mask must be located outside the chamber. $a >$ radius of chamber ~ 0.7 m.

The appropriate values for $a, b,$ and m can be obtained. They are $a = 1.00$ m, $b = 1.59$ m, $m = 0.0242$ inch. Also note that $d = 0.0625$ inch is a fixed value.

3.4 Metal box of photodiode arrays construction

In this section, the construction of metal box for holding 48 arrays of photodiode will be discussed. First the rough 2-view drawing for metal box was made. It is as shown in figure 21. The drawing must include 48 BNC ports for each channel of photodiode. Additionally, a circuit board drawing was also drawn as shown in figure 22(d). Then it was ordered online to hold the photodiodes.

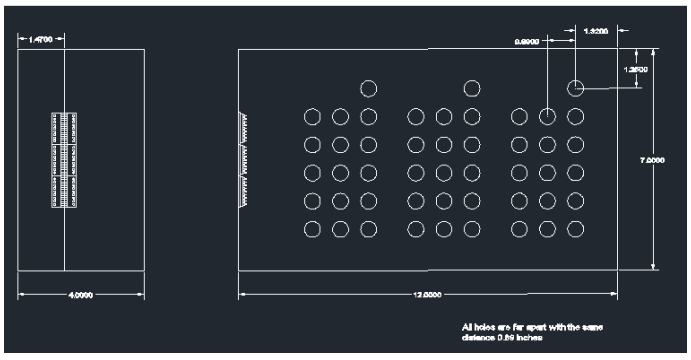

Figure 21: Drawing of aluminum box of size 4x7x12 inches to mount photo-detectors

After the drawings were approved, we then start to construct the box. Next, all the channels need to be connected to a pin of photodiode. This can be done by soldering wires to connect them as demonstrated in figure 22(c). The final picture of the box is shown in figure 22(a).

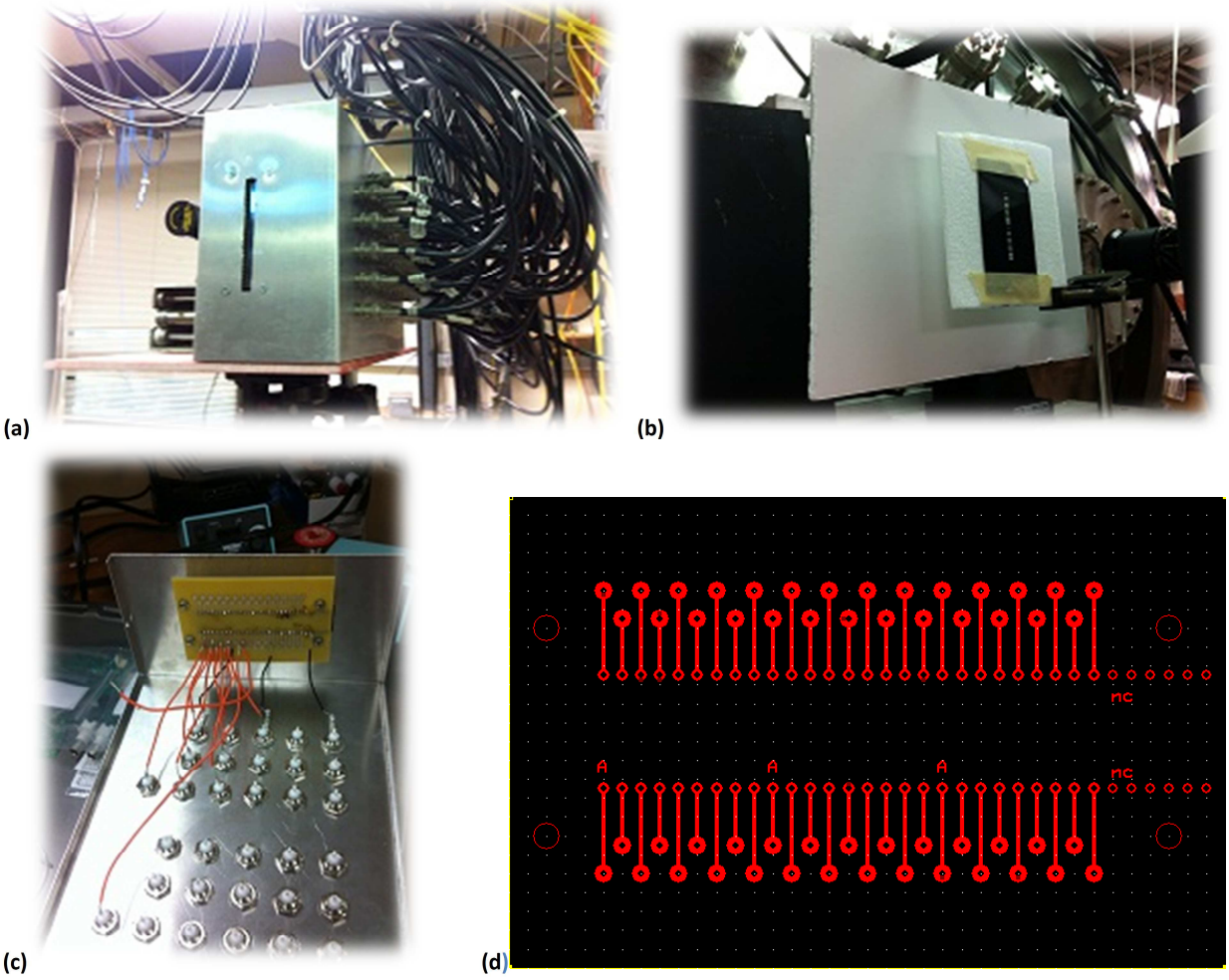

Figure 22: (a) finished metal box (b) mask (c) soldering process when constructing the metal box (d) drawing of the circuit board

4. Acknowledgement

I would like to thank Dr. Paul Bellan, my mentor, for providing me the opportunity to work under his direction this past summer. I thank all members of Bellan research group for their insight and guidance: Dave Felt, Xiang Zhai, Kilbyoung Chai, Vernon Chaplin, Bao Ha, Zachary Tobin, Mark Kendall, and Connie Rodriguez. Finally, I wish to thank Professor Bellan again and Caltech SURF program to financially support this project.

5. References

Accorsi, Roberto. *Design of Near-Field Coded Aperture Cameras for High-Resolution Medical and Industrial Gamma-Ray Imaging.* Cambridge, Massachusetts: MIT, 2001.

Akcasu, A. Z., R. S. May, G. F. Knoll, W. L. Rogers, K. F. Koral, and L. W. Jones. "Coded Aperture Gamma-Ray Imaging with Stochastic Apertures." *Opt. Engin. 13*, 1974: 117.

Baumert, L. D. "Construction of PN sequences." In *Digital Communications with Space Applications*, by S. W. Golomb, L. D. Baumert, M. F. Easterling, J. J. Stiffler and A. J. Viterbi, 165. Englewood Cliffs, New Jersey: PRENTICE-HALL, INC., 1964.

Dicke, R. H. "Scatter-hole cameras for X-rays and Gamma rays." *Astrophysical Journal 153*, 1968: L101.

Fenimore, E. E., and T. M. Cannon. "Coded aperture imaging with uniformly redundant arrays." *Applied Optics*, 1978: 337.

Golomb, Solomon W. *Digital Communications with Space Applications.* Englewood Cliffs, N.J.: PRENTICE-HALL, INC., 1964.

Koral, K. F., W. L. Rogers, and F. G. Knoll. "Digital tomographic imaging with time-modulated pseudorandom coded aperture and Anger camera." *Nucl. Medicine 16*, 1975: 402.

Miyamoto, Sigenori. "Hadamard Transform X-ray Telescope." *Space Science Instrumentation 3*, 1977: 473.

Miyamoto, Sigenori, Hiroshi Tsunemi, and Katsuhiko Tsuno. "Some Characteristic of the Hadamard Trasform X-ray Telescope." *Nuclear Instruments and Methods 180*, 1981: 557-572.

Nelson, E. D., and M. L. Fredman. "Hadamard Spectroscopy." *J. Opt. Soc. Am. 60*, 1970: 1664-1669.

Shutler, Paul M.E. "Signal-to-noise ratio in coded aperture imaging." *Nuclear Instruments and Methods in Physics Research A 669*, 2012: 22-31.

Accorsi, Roberto. *Design of Near-Field Coded Aperture Cameras for High-Resolution Medical and Industrial Gamma-Ray Imaging.* Cambridge, Massachusetts: MIT, 2001.

Akcasu, A. Z., R. S. May, G. F. Knoll, W. L. Rogers, K. F. Koral, and L. W. Jones. "Coded Aperture Gamma-Ray Imaging with Stochastic Apertures." *Opt. Engin. 13*, 1974: 117.

Baumert, L. D. "Construction of PN sequences." In *Digital Communications with Space Applications*, by S. W. Golomb, L. D. Baumert, M. F. Easterling, J. J. Stiffler and A. J. Viterbi, 165. Englewood Cliffs, New Jersey: PRENTICE-HALL, INC., 1964.

Dicke, R. H. "Scatter-hole cameras for X-rays and Gamma rays." *Astrophysical Journal 153*, 1968: L101.

Fenimore, E. E., and T. M. Cannon. "Coded aperture imaging with uniformly redundant arrays." *Applied Optics*, 1978: 337.

Golomb, Solomon W. *Digital Communications with Space Applications.* Englewood Cliffs, N.J.: PRENTICE-HALL, INC., 1964.

Koral, K. F., W. L. Rogers, and F. G. Knoll. "Digital tomographic imaging with time-modulated pseudorandom coded aperture and Anger camera." *Nucl. Medicine 16*, 1975: 402.

Miyamoto, Sigenori. "Hadamard Transform X-ray Telescope." *Space Science Instrumentation 3*, 1977: 473.

Miyamoto, Sigenori, Hiroshi Tsunemi, and Katsuhiko Tsuno. "Some Characteristic of the Hadamard Trasform X-ray Telescope." *Nuclear Instruments and Methods 180*, 1981: 557-572.

Nelson, E. D., and M. L. Fredman. "Hadamard Spectroscopy." *J. Opt. Soc. Am. 60*, 1970: 1664-1669.

Shutler, Paul M.E. "Signal-to-noise ratio in coded aperture imaging." *Nuclear Instruments and Methods in Physics Research A 669*, 2012: 22-31.

6. Appendices

6.1 Matlab code

```
% detector_box.m
%
% the code take signals saved from IDL code and then import here. For given
% shot_no, the code produces image of the signal detected by the detectors
% and image of deconstructed signal using inverse Hadamard transform.

clear all

shot_no = '13485';
folder = strcat('C:\Users\Pakorn\Documents\SURF\shots\',shot_no,'\');
% import file and save in V
for i = 1:48
    FID = fopen(strcat(folder,'Photodiode_ch',int2str(i),'_',shot_no,...
        '.dat'),'r');
    A = fread(FID,[8192,2],'float');
    V(:,i) = smooth(A(:,2),300);
    fclose(FID);
end

% reordering the channels
for i = 1:20
    Vc(:,i) = V(:,21-i);
    Vc(:,i+20) = V(:,41-i);
end
```

```
Vc(:,41:48) = V(:,41:48);
V = Vc;
t = A(:,1);

N = 47;
x = linspace(0,1,N)';

p =[0 1 1 1 1 ...
    0 1 1 1 1 ...
    0 0 1 0 1 ...
    0 1 1 1 0 ...
    0 1 0 0 1 ...
    1 0 1 1 0 ...
    0 0 1 0 1 ...
    0 1 1 0 0 ...
    0 0 1 0 0 ...
    0 0];       % PN-sequnce of period 47

M = p;

for i = 1:N-1
    M = [M;circshift(p,[0 i])];
end

H = -2*M+1;

t0 = 10;  % initial time
dt = 0.05; % time increment
nf = 1300; % number of frame
ti = t0:dt:t0+(nf-1)*dt;
for j = 1:nf
    Vi(j,:) = V(abs(t-ti(j)) < 1e-4,:);
    ti(j) = t0+(j-1)*dt;
end

Vi = Vi(:,1:47)';

F = -(2/(N+1))*(H)*Vi;  % Hadamard Transform

figure
subplot(1,2,1)
surf(ti,1:N,Vi*1e2)
axis equal
shading interp
view(0,90); % rotate to top view
colorbar
xlabel('time evolution (\mus)'); ylabel('position')
title('Detected signal')

subplot(1,2,2)
surf(ti,1:N,F*1e2)
axis equal
shading interp
view(0,90); % rotate to top view
colorbar
```

```
xlabel('time evolution (\mus)'); ylabel('position')
title('Original signal')

text(-20,70,strcat(('shot # '),num2str(shot_no)))
```
